Article citation info:
Szymański GM, Waligórski M, Misztal W. Assessment of the effectiveness of mounting the aircraft piston combustion engine on a test stand. Combustion Engines. 0000;XXX(X):xx-xx. https://doi.org/10.19206/CE-186702

Grzegorz M. SZYMAŃSKI
Marek WALIGÓRSKI
Wojciech MISZTAL

Combustion Engines
Polish Scientific Society of Combustion Engines

Assessment of the effectiveness of mounting the aircraft piston combustion engine on a test stand

ARTICLE INFO

Received: 11 December 2023
Revised: 2 April 2024
Accepted: 2 April 2024
Available online: 18 June 2024

The subject of the considerations described in the paper is the problem of the efficiency of mounting an aircraft engine on a dyno test bench. The paper presents the empirical research results of vibroacoustic signal application to the evaluation of the correctness of positioning of the Rotax 912 piston aircraft engine. The variability of selected parameters and vibroacoustic characteristics for real engine operating conditions was assessed, and functional relations and their discrete representations were developed, reflecting the efficiency of mounting the object on the frame. Thanks to this process, quantitative measures of the diagnostic assessment of the object were obtained, which can be used in periodic or continuous operational control of the object.

Key words: *aircraft engine, vibration isolation, mounting efficiency, empirical research, vibration accelerations-velocities-displacements*

1. Introduction

Empirical research on systems in which thermodynamic processes are carried out, characterized by high dynamics of changes in parameters and indicators of their operation, is conducted based on the assumptions of obtaining the most reliable measures and characteristics defining them [1, 4, 8]. Their purpose is not only the ongoing assessment of the quality of main processes, which is based on the analysis of the overall efficiency of the facility for specific operating conditions but also the process of generating and forecasting changes in operational characteristics with the time and intensity of use of the object in stationary and non-stationary conditions [22, 27, 28]. Thanks to this, it is possible to fill the multidimensional working space of the object with the representation of processes of a specific nature and properties observed there. The result is a more complete description of the mathematical behavior of the machine in real conditions of its operation, including conditions of conscious modification within the parameters of the system state vector, a control vector or an operational vector.

Regardless of the research objectives and evaluation criteria as well as limiting conditions (internal and external), the primary action of the scientific approach to research on modern systems is to ensure the most faithful representation of the course of dynamic processes in operating and accompanying parameters, such as in the case of mapping: rotational speed or valve clearance of the engine in its vibration equivalent [2, 7], identification of specific vibration parameters during the process of transporting ingredients of the feeding process [14] or bearing lubrication conditions [15], assessment of thermodynamic processes occurring in turbojet or piston engines [29, 33], the impact of a specific fuel on the efficiency of the combustion process and emissions of harmful exhaust gas components [18–20, 36]. This is particularly important in the case of diagnosis using vibroacoustic processes, which may have different partial goals and application areas, such as: searching for the most effective method of reducing the number of parameters used to evaluate [23], using vibrations to assess the operation of multi-stage wind turbine gearboxes [24, 35], methodology for research process depending on the type of process and its nature [26], taking into account safety criteria in the diagnostic assessment [30], using the process of optimizing structures and systems with high dynamics of changes in thermodynamic processes [37]. The active value of the measurement signal and its effectiveness in describing the observed partial process is also dependent on the quality of mounting the engine on the test stand, the issue of which is very important and its importance is greater the more complex the structure of the object and the correlation between its various parameters are.

In order to reduce vibration amplitudes in technical facilities where dynamic processes are carried out, it is necessary to use appropriate methods to reduce their movement between the source of vibrations and the object absorbing vibroacoustic energy [9]. For this purpose, an intermediate element or system is used, thanks to which the value of the above energy is reduced or even the value of the vibration amplitude is completely dampened (a vibration isolator). The phenomenon of decreasing the amplitude of vibrations when passing from their source to the receiver is called vibroisolation. In the case of modeling mechanical systems in which a vibration isolator is used, their linearity (the superposition of effects) and stationarity are assumed, and the interactions between them are treated as determined or stationary random processes. Thanks to this, the analysis of excitations and their mathematical description can be carried out using frequency analyzes and in the field of system properties (transmittances as system characteristics regarding a susceptibility). In reality, the connections between the source, the vibroisolator and the receiver of vibroacoustic energy are multi-point or surface (modeling of extended finite systems or discrete matrix models). Minimization of vibration amplitudes can be achieved by separating dynamic forces from the isolated area (force vibration isolation), or by

reducing dynamic displacements of the vibration-sensitive system (displacement vibration isolation) [5, 16, 17].

An object generating mechanical vibrations is a source of dynamic force from the process occurring within it. This machine is placed on a supporting structure. If its vibrations exceed the permissible values, the source of these exceedances is too high a resultant dynamic force is transferred from the machine to the supporting frame and inappropriate selection of the properties of the subsystems (a source, a vibration isolator, a vibration receiver). In order to reduce the force transmitted to the frame of the supporting structure, the dynamic system should be compared without and with a vibroisolator, using the appropriate susceptibility matrices α^0 i α (after applying the insulation, Fig. 1).

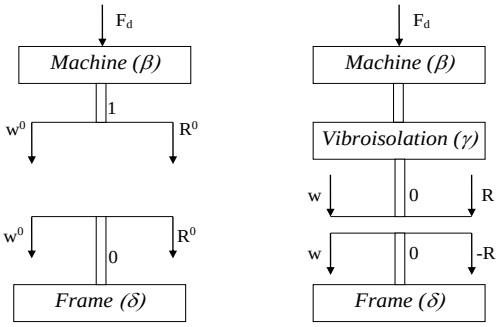

Fig. 1. General diagram of the definition of force vibration isolation [5]

The effectiveness of vibration isolation can be defined by the following equation [5, 16]:

$$E_{WI} = \left|\frac{R^0}{R}\right| = \left|\frac{w^0}{w}\right| > 1 \tag{1}$$

where: R^0 – force transmitted to the supporting structure for the system without a vibration isolator, R – force transferred to the supporting structure for the system with a vibroisolator (value after passing through the isolator), w^0 – displacement for a system without a vibration isolator, w – displacement for a system with a vibroisolator (after passing through the vibroisolator).

If the displacements from eq. (1) are expressed by the susceptibility as the amplitude of the response to the unit harmonic excitation at point i, measured at point j as [5]:

$$w^0 = -\delta_{00}R^0 \tag{2}$$

$$w = -\delta_{00}R \tag{3}$$

where: δ_{00} – susceptibility of the frame structure at the point of contact with the insulator
then the following relationship is obtained after taking into account the properties of the systems, in accordance with the susceptibility method:

$$w^0 = \alpha_{k0}^0 F_d = \frac{\delta_{00}\beta_{k1}}{\beta_{11}+\delta_{00}} F_d \tag{4}$$

$$w = \alpha_{k0} F_d = \frac{\gamma_{10}\delta_{00}\beta_{k1}}{(\delta_{00}+\gamma_{00})(\beta_{11}+\gamma_{11})-\gamma_{10}^2} F_d \tag{5}$$

where: α^0 – susceptibility matrix for a system without vibration isolation, α – susceptibility matrix for a system with vibration isolation, F_d – value of the force from the source of excitation, γ_{00}, γ_{11}, γ_{10} – susceptibility of the machine and the foundation (a primary connection), and on the direct and cross-impact susceptibility of the isolator, β – machine susceptibility for a specified side.

By transforming equations (4) and (5), the final dependency on the effectiveness of vibration isolation is obtained in the form [5]:

$$E_{WI} = \left|\frac{\alpha_{k0}^0}{\alpha_{k0}}\right| = \left|\frac{(\delta_{00}+\gamma_{00})(\beta_{11}+\gamma_{11})-\gamma_{10}^2}{(\beta_{11}+\delta_{00})\gamma_{10}}\right|, \tag{6}$$

The assessment of the effectiveness of vibration isolation depends on the susceptibility of the machine and the foundation (a primary connection) and on the direct and cross-impact susceptibility of the isolator γ_{00}, γ_{11}, γ_{10}.

In the case of displacement vibration isolation (Fig. 2), the goal is to provide vibration protection to a system with a susceptibility matrix β located on a foundation with properties δ. The source of forcing F_d determines the vibrations of the foundation, and the effectiveness of their isolation is equal to [5]:

$$E_z = \left|\frac{z}{w}\right| = \left|\frac{\alpha_{k0}^0}{\alpha_{k0}}\right| > 1 \tag{7}$$

where: z – displacement for a system without a vibration isolator, w – displacement for a system with a vibration isolator (before the isolator).

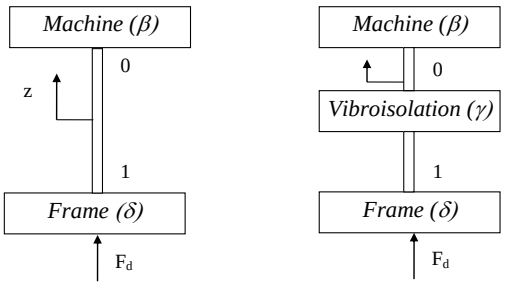

Fig. 2. Diagram of displacement vibration isolation definition [5]

Analysis using the susceptibility method allows obtaining the appropriate value for the primary system and the system with a vibroisolator:

$$\alpha_{k0}^0 = \frac{\beta_{11}\delta_{k0}}{\delta_{00}+\beta_{11}} \tag{8}$$

$$\alpha_{k0} = \frac{\beta_{11}\delta_{k0}\gamma_{10}}{(\beta_{11}+\gamma_{11})(\delta_{00}+\gamma_{00})-\gamma_{10}^2} \tag{9}$$

Substituting the above equations into the formula (7), the equation for the effectiveness of a displacement vibration isolation is given as [5]:

$$E_z = \left|\frac{z}{w}\right| = \left|\frac{\alpha_{k0}^0}{\alpha_{k0}}\right| = \left|\frac{(\beta_{11}+\gamma_{11})(\delta_{00}+\gamma_{00})-\gamma_{10}^2}{(\delta_{00}+\beta_{11})\gamma_{10}}\right| \tag{10}$$

The mathematical relationships obtained for the force and displacement vibration isolations are equal. Depending on needs, one can use force or displacement vibration isolation systems. In the case of the force isolation on a rigid foundation, it is equivalent to the displacement isolation for a kinematic forcing. In assessing the effectiveness of a system isolation from mechanical vibrations, the dynamic

properties of the component systems are undoubtedly important. If no external energy is supplied, then these systems have passive elements, which makes the vibration isolator is a symmetrical mechanical system (the susceptibility at the beginning is equal to its value at the end). In the low frequency range, the properties of the vibration isolator are elastic, so the isolation will take place if the susceptibility of the insulator (1/k, where k – isolator stiffness) will be greater than the absolute value of the sum of the susceptibilities of a machine β_{11} and a frame structure δ_{00}. Thanks to this, it is possible to conclude what dynamic characteristics of the machine and foundation should be used in the above assessment. The above parameters can also be obtained based on empirical research.

If the direct susceptibility of the isolator is much greater than that of the machine or a foundation, then [5]:

$$\left|\frac{\delta_{00}}{\gamma_{11}}\right| \ll 1, \left|\frac{\beta_{11}}{\gamma_{11}}\right| \ll 1 \tag{11}$$

and therefore:

$$E = \left|\frac{\gamma_{11}^2-\gamma_{10}^2}{(\beta_{11}+\delta_{00})\gamma_{10}}\right| \gg 1 \tag{12}$$

hence:

$$\left|\frac{\gamma_{11}^2-\gamma_{10}^2}{\gamma_{10}}\right| \gg |(\beta_{11}+\delta_{00})| \tag{13}$$

The conditions defined by the inequalities in (13) are not met if the absolute value of γ_{11} is close to 0. These conditions are met for an elastic isolator, hence the mutual susceptibility γ_{10} is important. In this case, the best vibration isolation is provided by a symmetrical isolator in which $|\gamma_{11}| >> 1$ and $|\gamma_{10}| \approx 0$. The susceptibility of the isolator also depends on the frequency. The above inequality will be fulfilled if the resonance value in the direct susceptibility is significantly greater than the mutual susceptibility. The issues of vibration isolation of systems require further detailed studies and empirical research, especially in the context of the development of materials engineering, regarding e.g.: nanoparticles and composite structures [3, 6], coating on fiber insolation of thermal and vibration processes [10, 21], external composite systems [25], acoustic metamaterials for low-frequency broadband vibration and sound insulation [31, 32], composites structures studied for specified boundary conditions [34].

Taking into account the problems related to the incorrectly selected type and design of a vibroisolator for a given machine (damage to the structure, occurrence of resonant vibrations), the following research goal was formulated: to assess the effectiveness of the designed vibroisolator for an aircraft piston engine placed on a dynamometer test stand.

2. Research methodology

The research was carried out based on the author's development methodology for empirical tests of engines in bench conditions. The research methodology was based on the passive experiment. The engine speed and torque were chosen as the input parameters. Vibration accelerations of the engine block and engine frame were taken into consideration as the output parameters.

The accelerometers were put on the engine block and the engine frame. Such a position was selected to obtain a high vibration signal sensitivity regarding the observed process and a low sensitivity to the other vibrations. Placements and orientations of the accelerometer on the engine block and frame were considered. The optimal positions for the transducers were selected based on the analysis of the dynamic process related signal to noise ratio. The research dimensions of digital signals were chosen as: X dimension – parallel to the cylinder axis (and perpendicular to the frame surface), Y dimension – parallel to the frame surface and perpendicular to the crankshaft axis, Z dimension – parallel to the crankshaft axis and perpendicular to the cylinder axis.

Values of the engine speed and load were selected within the engine operative area. Digital data was sampled during experiments once coolant and temperatures were stabilized. Software algorithms were developed by the authors and were used to manage the data post-processing analysis. The sampling frequency during the research process was 65,536 Hz for each channel of the measurement system.

Measurement of selected parameters of the vibroacoustic process for specific engine performance was carried out following the principle of finding a reliable diagnostic parameter for accurate evaluation of the effectiveness of mounting the aircraft piston combustion engine on a test stand.

3. Engine test stand and research equipment

All researches were performed for the engine test stand conditions, and the working points of the engine were chosen from the engine speed and torque operating ranges (Fig. 3, 4).

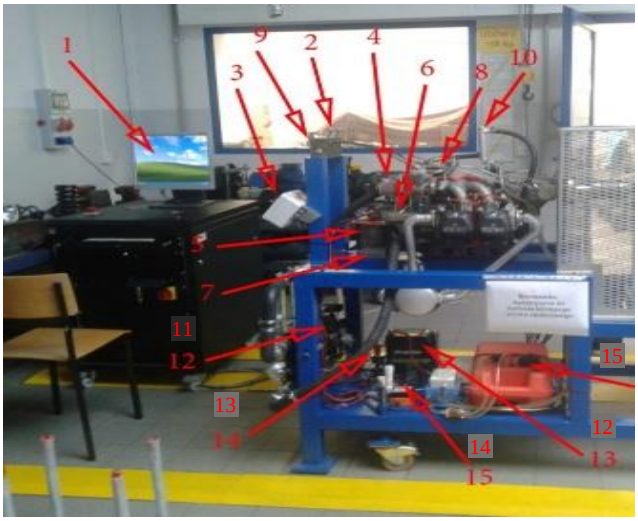

Fig. 3. The view and components of the test stand: 1 – computer, 2 – throttle and choke levers, 3 – desktop, 4 – air filter, 5 – oil tank, 6 – starter, 7 – regulator, 8 – magnetos, 9 – oil pressure gauge, 10 – oil cooler, 11 – coolant radiator, 12 – battery, 13 – main power switch, 14 – electromagnet, 15 – fuel tank

The research was carried out using a six-channel measurement system with a B&K LAN-XI type 3050-A-060 card (possibility of parallel recording with a band frequency of up to 51.2 kHz) – Table 1, Fig. 4.

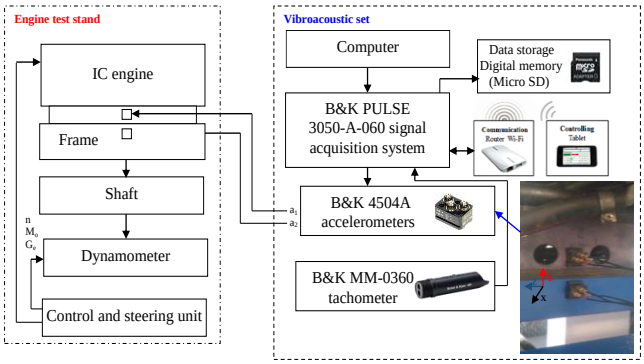

Fig. 4. The scheme of the measurement circuit connections and installation of vibration transducers to the engine and frame

Table 1. The technical specification of a LAN-XI 3050-A-060 [12]

B&K LAN-XI 3050-A-060	
Number of channels	6
Frequency passband [Hz]	1–51200
DC input [V DC]	10–32
Temperature range [°C]	–25–70
Absolute amplitude precision, 1 kHz, 1 V_{input}	±0.05 dB, typ. ±0.01 dB
Amplitude linearity	±0.01–0.02 dB (from 0–140 dB)
Weight [g]	750
Output	CCLD/microphone preamplifier (0 or 200 V polarization voltage), charge
Data handling	16 GB SD card (4 h of recording with 6 channels at 25.6 kHz bandwidth

The recorded signals and the obtained results were observed on a computer screen using the PULSE Reflex Core software. Vibration acceleration measurements were carried out using two three-axis piezoelectric transducers of the B&K 4504A type (Table 2). The above accelerometers were calibrated separately for each measurement axis. Aluminum housing and lead piezoelectric element, DC power supply and high resonance frequency are some of the advantages of the transducer, thanks to which the transducer's low weight, high sensitivity and low sensitivity to external factors (including environmental factors) are achieved.

Table 2. The technical specification of a Bruel&Kjær 4504A accelerometer [12]

Bruel&Kjær 4504A	
Frequency [Hz]	1–10,000
Senitivity [mV/g]	10
Temperature range [°C]	–50–125
Residual noise level in spec. freq. range (RMS) [mg]	±0.4
Maximum operational/shock level (peak) [g]	±750/±3000
Weight [g]	15
Output	CCLD
Resonance frequency [kHz]	50
Triaxial/TEDS/Electrical connector	Yes/No/10-32 UNF

The placements of the vibration acceleration transducers (Bruel&Kjær 4504A) were located on the engine block and the engine frame, nearby generated dynamic processes. Measurements were done for 3 perpendicular dimensions, and the recorded cyclic processes were defined using an angle encoder B&K MM0360 (Table 3).

Table 3. The technical specification of the B&K MM0360 angle encoder [12]

Feature \ Sensor	
Transducer type	MM0360
Velocity range [rpm]	0–300,000
Operating range	1.5 (0.6) to > 70 cm (27") and > 30° from centre line
Laser spot	< ∅5 mm at 70 cm distance
Maximum continuous input voltage [V]	–5 to +30
Laser class	3R. Visible 660–690 nm, CW, P [optical] < 2 mW. Complies with EN/IEC 60825-1:2007
Temperature range [°C]	–10 to +50
Input type	CCLD (DeltaTron or ICP® inputs from 3 to 20 mA), U ≥ 20V

4. Research engine

A spark-ignition internal combustion engine of the Rotax 912 type was used as the research object. The above-mentioned four-cylinder naturally aspirated engine is a design with a counter-rotating arrangement of cylinders (boxer type), in which there are two carburetors (BING) with a central fuel chamber (supplied by a mechanical fuel pump), and the pressure lubrication system (with the so-called dry sump) has 2 oil pumps and an oil cooler. This engine has a mixed cooling system, where the cylinders are cooled by air and the heads by liquid (the liquid pump is driven by a gear transmission from the engine's crankshaft). Each head is equipped with two valves (intake, exhaust) hydraulically controlled, with the possibility of adjusting valve clearances (Fig. 5).

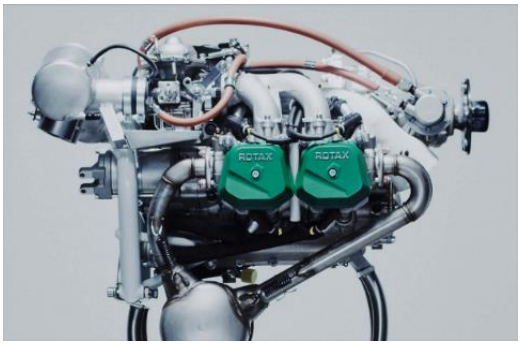

Fig. 5. The view of the Rotax 912 engine [13]

Table 4. Operating and geometric parameters of the Rotax 912 engine [11]

Parameter type	Value
Rated effective power [kW]	59.6 (at 5800 rpm)
Engine displacement [cm^3]	1211
Cylinder diameter/piston stroke [m/m]	0.0795/0.0610
Compression ratio [–]	9.1
Fuel consumption [dm^3/h]	15.0 (by 5000 rpm in 75% of rated effective power)
Mass power coefficient [kW/kg]	0.98
Engine length/width [m/m]	0.561/0.576
Engine mass [kg]	60

5. Research conditions

Empirical research was done under the following research conditions:

- ambient conditions at the engine test stand area: t_o = = 20°C and p_o = 1012 hPa
- operating conditions: stationary, for each constant engine speed value and constant torque (7 engine speed values from the range 700–1400 rpm) and the torque values were 0 Nm (Table 5)
- vibroacoustic conditions: vibration acceleration passband range: 1–24,000 Hz, sampling rate: 65.536 kHz
- placement of a vibration transducer: first on the engine block (recording in the 3 perpendicular directions) and second at the engine frame (3 perpendicular directions).

Table 5. The reproduction of stand operating conditions and recorded vibroacoustic parameters carried out in the research program

Operating conditions		Recorded parameters	
n [rpm]	M_o [N·m]	Engine block	Engine frame
700	0	$a_{x,block}$ $a_{y,block}$ $a_{z,block}$	$a_{x,frame}$ $a_{y,frame}$ $a_{z,frame}$
900			
1000			
1100			
1200			
1300			
1400			

Obtained vibration accelerations were directed to the analog inputs of the acquisition card. Signals were filtered in the card (by analog and digital filters) and were converted from analog to digital form, which were stored in a computer memory then. The recorded all-time history courses of the signals were subjected to the time selection process, in which all recorded signals were divided into signal sequences including single IC engine working cycles.

The rotational speed values were measured using an angle encoder placed after the reducer, therefore, to obtain the rotational speed on the engine crankshaft, the following equation had to be used:

$$n_e = 2.27 \cdot n \tag{14}$$

where: 2.27 – geometric transmission ratio of the reducer, n_e – the engine crankshaft speed [rpm], n – the rotation speed measured after the reducer [rpm].

6. Measurement results

6.1. Assessment of the effectiveness of vibration isolation of the engine mounting

The correctness of the selection of vibration isolating elements is assessed based on the measurement of vibration signals before and after the vibration isolator. Figure 6 shows the time history of vibration acceleration signals recorded on the engine and on the frame of the test stand (in two perpendicular directions).

Based on the analysis of Fig. 6, it can be concluded that the maximum vibration acceleration amplitudes have decreased for both directions of vibration measurement. The vibration acceleration signals were analyzed by calculating the damping coefficient based on the eq. (10). The analysis results regarding the maximum vibration acceleration values are presented in Table 6.

Table 7 presents the results of analyzes regarding vibration damping in the energetic sense, based on the values of the RMS vibration accelerations.

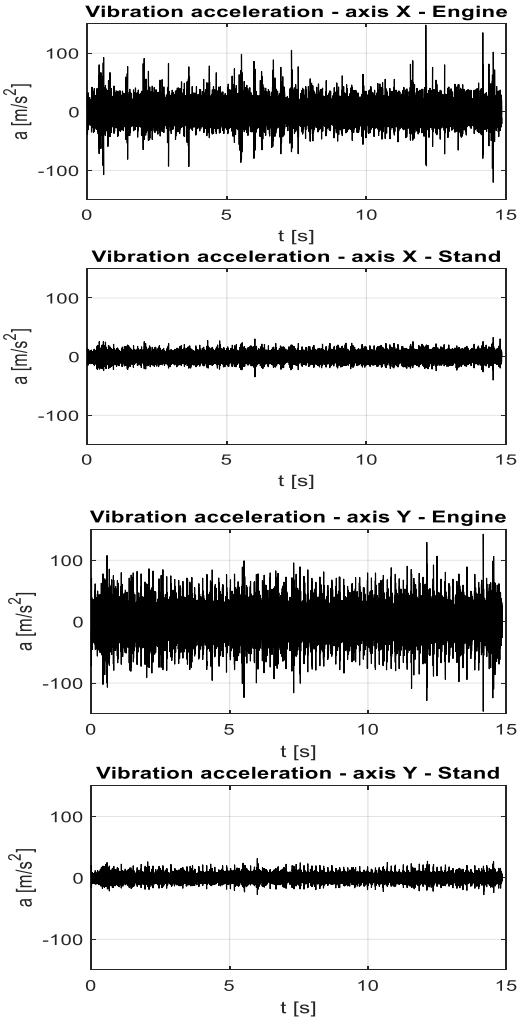

Fig. 6. The time history of vibration acceleration for two measurement points and two orthogonal directions

Table 6. The list of damping coefficients of vibration acceleration signal parameters regarding maximum values

n [rpm]	Vibration acceleration damping [–]	
	X axis	Y axis
700	3.70	4.63
900	3.46	4.65
1000	4.33	6.18
1100	2.73	4.90
1200	2.79	2.95
1300	3.47	6.03
1400	3.01	3.27

Table 7. The list of damping coefficients of vibration acceleration signal parameters in terms of energy (for the RMS estimator)

n [rpm]	Vibration acceleration damping [–]	
	X axis	Y axis
700	1.82	3.58
900	1.83	3.58
1000	2.36	4.81
1100	2.27	3.47
1200	2.21	3.88
1300	2.08	4.06
1400	2.27	2.69

Based on the analysis of the damping coefficients listed in Table 6 and Table 7, it was found that for all engine operation settings during the tests, the vibration acceleration signals were damped.

Figure 7 shows the time history of vibration velocity signals recorded on the engine and on the frame of the test stand (in two perpendicular directions).

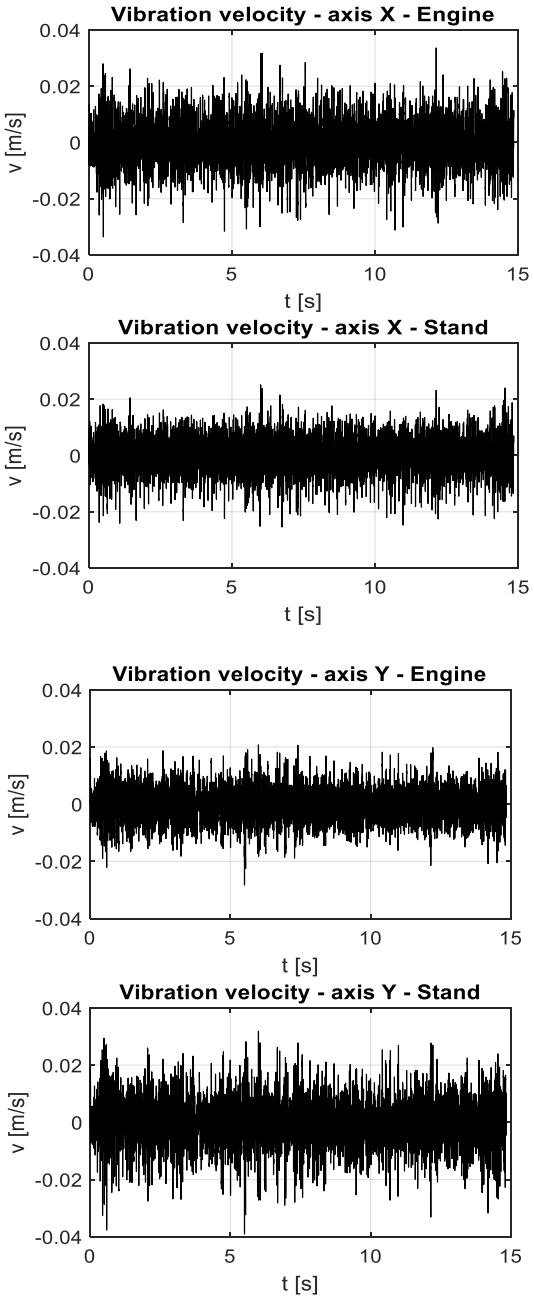

Fig. 7. The time history of vibration velocity for two measurement points and two orthogonal directions

Based on the analysis of Fig. 7, it can be concluded that the maximum vibration velocity amplitudes were reduced in the X direction, while they were strengthened in the Y direction. The vibration velocity signals were analyzed by calculating the damping coefficient. The analysis results regarding the maximum vibration acceleration values are presented in Table 8.

Table 8. The list of damping coefficients of vibration speed signal parameters regarding maximum values

n [rpm]	Vibration velocity damping [–]	
	X axis	Y axis
700	1.32	0.72
900	1.22	0.64
1000	1.26	0.74
1100	1.37	0.58
1200	1.01	0.72
1300	1.36	0.65
1400	1.31	0.66

Table 9. The list of damping coefficients of vibration speed signal parameters in terms of energy (for the RMS estimator)

n [rpm]	Vibration velocity damping [–]	
	X axis	Y axis
700	1.29	0.60
900	1.33	0.53
1000	1.20	0.62
1100	1.35	0.54
1200	1.19	0.69
1300	1.37	0.66
1400	1.29	0.62

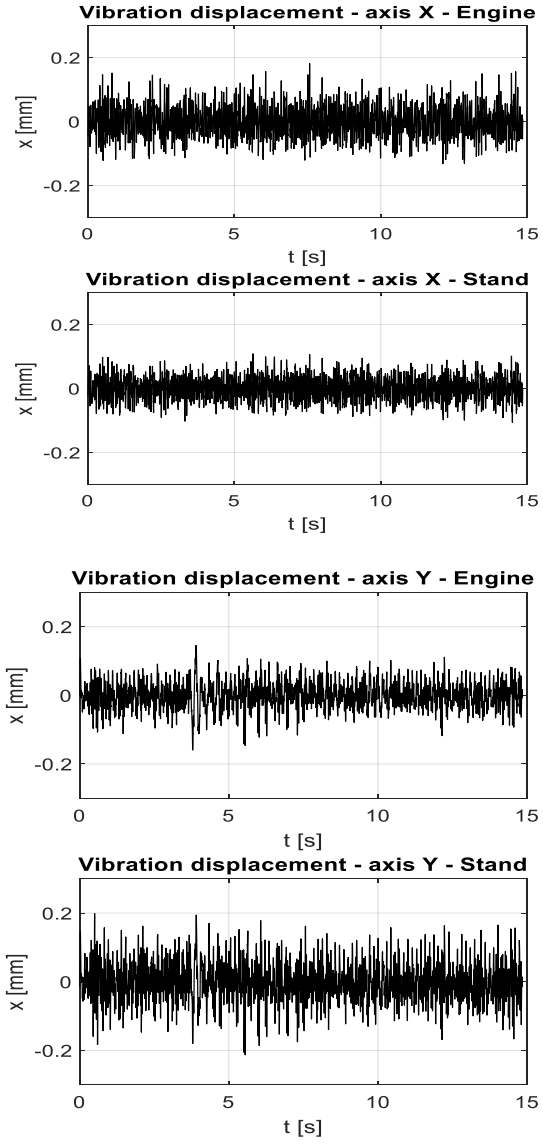

Fig. 8. The time history of a vibration displacement for two measurement points and two orthogonal directions

Table 9 presents the results of analyzes regarding vibration damping in the energetic sense, based on the values of RMS vibration velocities.

Based on the analysis of the damping coefficients listed in Table 8 and Table 9, it was found that for all engine operation settings during the tests, the vibration speed signals were damped in the X direction and strengthened in the Y direction.

In a similar way, the effectiveness of damping vibration displacements was analyzed, the time history of which is presented in Fig. 8. It was found that the maximum amplitudes of vibration displacements were reduced in the X direction, and strengthened in the Y direction.

The vibration displacement signals were analyzed by calculating the damping coefficient. The results of the analyzes regarding the maximum values of vibration acceleration are presented in Table 10, and the results of calculations regarding vibration damping in the energy sense, based on the values of effective vibration velocities, are presented in Table 11.

Table 10. The list of damping coefficients of vibration displacement signal parameters regarding maximum values

n [rpm]	Vibration displacement damping [–]	
	X axis	Y axis
700	1.67	0.75
900	1.49	0.63
1000	1.40	0.81
1100	1.71	0.71
1200	1.62	0.66
1300	1.90	0.55
1400	1.58	0.56

Table 11. The summary of the results of attenuation of vibration displacement signal parameters in terms of energy (for the RMS estimator)

n [rpm]	Vibration displacement damping [–]	
	X axis	Y axis
700	1.34	0.69
900	1.25	0.61
1000	1.13	0.69
1100	1.31	0.57
1200	1.30	0.66
1300	1.65	0.59
1400	1.83	0.53

Based on the analysis of the damping coefficients listed in Table 10 and Table 11, it was found that for all engine operation settings during the tests, the vibration displacement signals were damped in the X direction and strengthened in the Y direction.

6.2. Frequency analysis

Since the broadband analysis was not clear, a frequency analysis was performed to explain the discrepancies between the results of the calculated damping coefficients for accelerations, velocities and vibration displacements, especially in the Y direction.

Figure 9 shows the amplitude spectra of the vibration acceleration signals recorded at different rotational speed settings of the propeller shaft. It was found that for the presented engine operation settings, the spectra are of a similar nature, i.e. they differ in amplitudes for similar frequencies. With this in mind, the rest of the article presents the analysis results for measurements at a propeller shaft rotation speed of 700 rpm.

Figure 10a,c,e compares the spectra of accelerations, velocities and vibration displacements in the entire recorded frequency band (for the engine and the stand frame in the X direction), while Fig. 10b,d,f shows a comparison of spectra for the same conditions only in the 4–200 Hz band, which corresponds to the first five rotational harmonics of the engine crankshaft.

The analysis of the results presented in Fig. 10 allows for the following conclusions to be drawn regarding the effectiveness of vibration isolation in the X direction in the case of:

- vibration acceleration, and damping occur in most of the frequency range except for the following bands: 65–75 Hz, 145–200 Hz, 270–720 Hz, 1200–2000 Hz. The greatest attenuation occurs at higher frequencies above 2 kHz
- vibration speeds, the amplification occurs only in the band: 65–75 Hz
- vibration displacements, and damping occur for the entire range of analyzed frequencies.

A comparison of the spectra of accelerations, velocities and vibration displacements in the entire recorded frequency band (for the engine and the stand frame in the Y direction) is shown in Fig. 11a,c,e, while Fig. 11b,d,f shows a comparison of spectra for the same conditions only in the 4–200 Hz band, which corresponds to the first five rotational harmonics of the engine crankshaft.

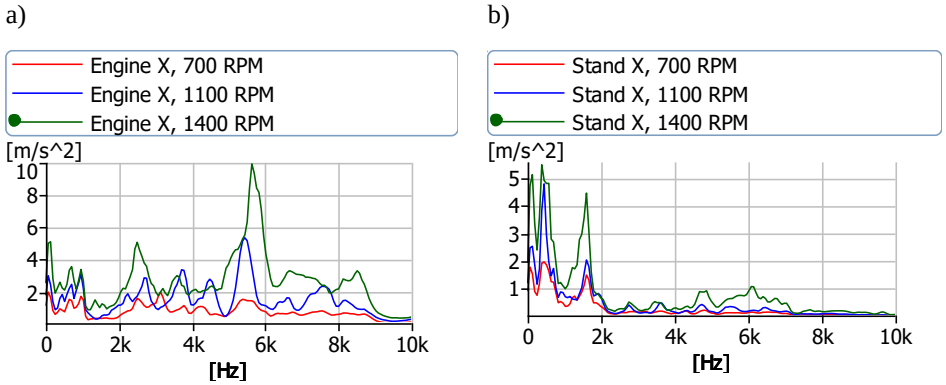

Fig. 9. The amplitude spectra of vibration accelerations at different shaft rotational speed settings recorded on: a) the engine, b) the frame of a test stand

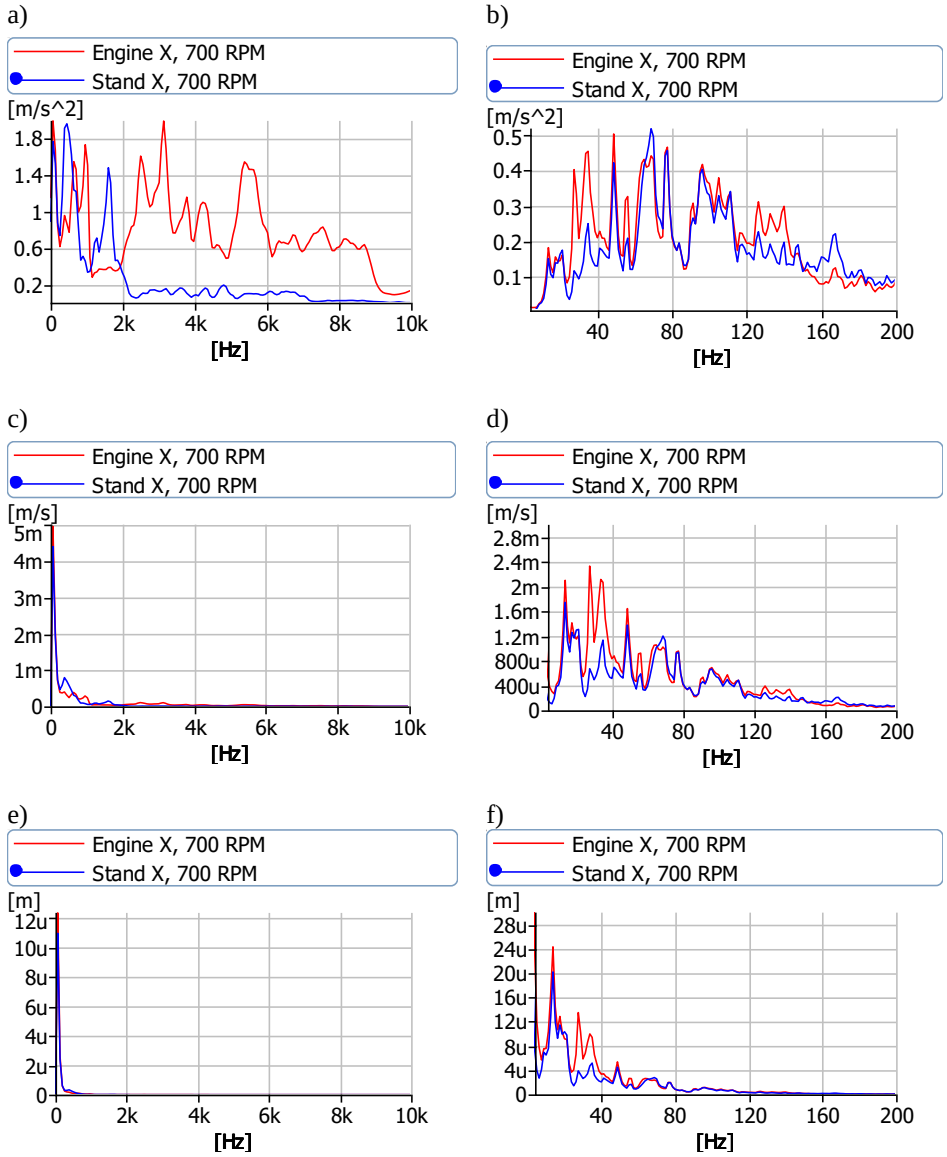

Fig. 10. The spectra of signals in the X direction: a, c, e) accelerations, velocities and vibration displacements in the entire recorded frequency band and b, d, f) accelerations, velocities and vibration displacements in the 4–200 Hz band (m – mil, u – micro)

Based on the analysis results presented in Fig. 11, the following conclusions were made regarding the effectiveness of vibration isolation in the Y direction in the case of:

- vibration accelerations, the damping occurs at frequencies above 500 Hz, while the vibration amplification is observed at frequencies lower than 500 Hz
- vibration velocities, the damping and amplification occur in the same frequency ranges as in the case of vibration accelerations
- vibration displacements, the amplification occurs for the entire range of analyzed frequencies.

Conclusions

The presented work is based on empirical research carried out by its authors within the study of the effectiveness of mounting the aircraft piston combustion engine on a test stand.

The analysis of damping effectiveness carried out in the amplitude domain using dimensional point measures such as peak value and RMS, based on the determination of the damping coefficient for the X and Y directions and various engine rotation speeds, confirmed the damping effectiveness in the case of vibration accelerations for both recorded directions of the measurement signal. In the case of vibration speed only in the X direction, reductions in the peak vibration amplitude and their RMS values were observed. A similar situation occurred for vibration displacements. Hence, the analysis was supplemented with those carried out in the frequency domain.

In the case of the frequency domain assessments, the effectiveness of vibration isolation for vibration acceleration in the X direction was proved in most of the frequency range (except 65–75 Hz, 145–200 Hz, 270–720 Hz, 1200–2000 Hz). The greatest vibration decrease occurred at frequencies above 2 kHz. In the case of vibration speeds, the amplification occurs only in the band 65–75 Hz, and for vibration displacements damping occurs for the entire range of analyzed frequencies.

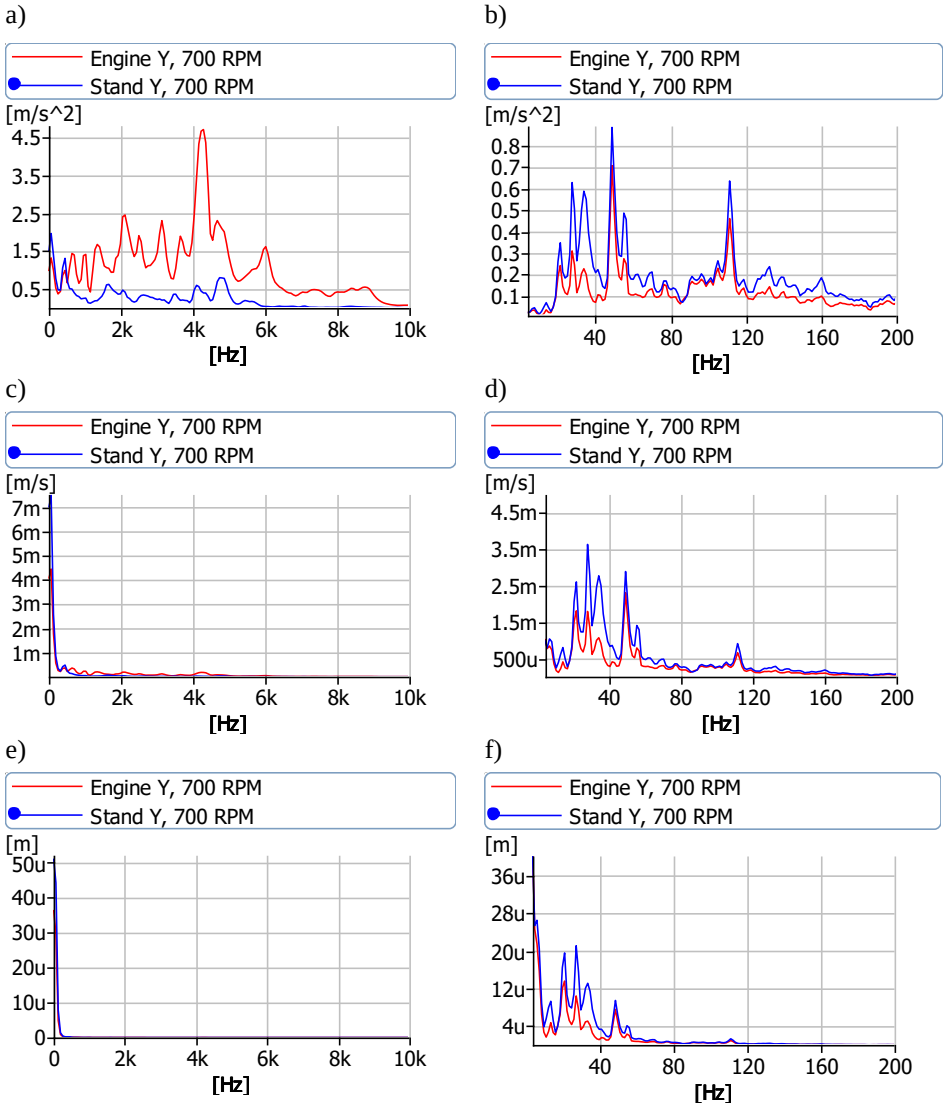

Fig. 11. The spectra of signals in the Y direction: a, c, e) accelerations, velocities and vibration displacements in the entire recorded frequency band and b, d, f) accelerations, velocities and vibration displacements in the 4–200 Hz band (m – mil, u – micro)

In the case of vibration accelerations in the Y direction, the damping occurs at frequencies above 500 Hz, while the vibration amplification is observed at frequencies lower than 500 Hz. The same situation occurred in the case of vibration velocities. The amplification occurs for the entire range of analyzed frequencies for vibration displacements.

Acknowledgements

This work was partly supported by Polish Ministry of Education and Science fund for Statutory Activities of: the Institute of Combustion Engines and Powertrains, PUT (PL) 0415/SBAD/0342, and the Institute of Transport, PUT (PL) 0416/SBAD/0005.

Nomenclature

a_1	vibration accelerations obtained from the transducer placed at the engine block
a_2	vibration accelerations obtained from the transducer placed at the engine frame
$a_{x,block}$	vibration accelerations in X direction at the engine block
$a_{y,block}$	vibration accelerations in Y direction at the engine block
$a_{z,block}$	vibration accelerations in Z direction at the engine block
$a_{x,frame}$	vibration accelerations in X direction at the engine frame
$a_{y,frame}$	vibration accelerations in Y direction at the engine frame
$a_{z,frame}$	vibration accelerations in Z direction at the engine frame
CCLD	constant current line drive
E_{WI}	efficiency of force vibration isolation
E_z	efficiency of displacement vibration isolation
F_d	value of the force from the source of excitation
G_e	stream mass of fuel consumption

IC	internal combustion
m	mil
M_o	torque
n	rotation speed measured after the reducer
n_e	engine crankshaft speed
P	power
p_o	ambient pressure
R	force transferred to the frame structure for the system with a vibroisolator (value after passing through the isolator)
R^0	force transmitted to the supporting structure for the system without a vibration isolator
RMS	root mean square
SD	secure digital
TEDS	transducer electronic datasheet
t_o	ambient temperature
u	micro
U	voltage
w	displacement for a system with a vibration isolator (after passing through the vibration isolator)
w^0	displacement for a system without a vibration isolator
z	displacement for a system without a vibration isolator
α	susceptibility matrix for a system with vibration isolation
α^0	susceptibility matrix for a system without vibration isolation
β	machine susceptibility
δ	susceptibility of the frame structure
γ	vibration isolator susceptibility

Bibliography

[1] Arroyo J, Muñoz M, Moreno F, Bernal N, Monné C. Diagnostic method based on the analysis of the vibration and acoustic emission energy for emergency diesel generators in nuclear plants. Appl Acoust. 2013;74(4):502-508. https://doi.org/10.1016/j. apacoust.2012.09.010

[2] Avramchuk VS, Kazmin VP. Estimation of combustion engine rotation speed based on vibration signal analysis. KEM. 2016;685:436-440. https://doi.org/10.4028/www.scientific.net/kem.685.436

[3] Berberova-Buhova N, Nedelchev L, Mateev G, Stoykova E, Strijkova V, Nazarova D. Influence of the size of Au nanoparticles on the photoinduced birefringence and diffraction efficiency of polarization holographic gratings in thin films of azopolymer nanocomposites. Opt Mater. 2021;121: 111560. https://doi.org/10.1016/j.optmat.2021.111560

[4] Brzeziński K. Active-passive: on preconceptions of testing. Journal of Telecommunications and Information Technology. 2011;3:63-73. https://yadda.icm.edu.pl/baztech/element/bwmeta1.element.baztech-article-BAT8-0021-0008

[5] Cempel C. Vibroacoustic machines diagnostics. Polish Scientific Publishing Houses. Warsaw 1989.

[6] Chen Y, Li F. Analysis of vibration and sound insulation characteristics of functionally graded sandwich plates. Compos Struct. 2020;249:112515. https://doi.org/10.1016/j.compstruct.2020.112515

[7] Czechyra B, Szymański GM, Tomaszewski F. Assessment of cam valves clearance in internal combustion engine based on parameters of vibration – methodological assumption. Combustion Engines. 2004;118(1):51-59. https://doi.org/10.19206/CE-117424

[8] Delvecchio S, Bonfiglio P, Pompoli F. Vibro-acoustic condition monitoring of internal combustion engines: a critical review of existing techniques. Mech Syst Signal Pr. 2018; 99:661-683. https://doi.org/10.1016/j.ymssp.2017.06.033

[9] Fiebig W, Wróbel J. Two stage vibration isolation of vibratory shake-out conveyor. Arch Civ Mech Eng. 2017; 17(2):199-204. https://doi.org/10.1016/j.acme.2016.10.001

[10] He D, Ou D, Gao H, Jiao F. Thermal insulation and anti-vibration properties of $MoSi_2$-based coating on mullite fiber insulation tiles. Ceram Int. 2022;48(2):1844-1850. https://doi.org/10.1016/j.ceramint.2021.09.267

[11] https://www.altair.com.pl/news/view?news_id=3780 (accessed on 17.12.2009).

[12] https://www.bksv.com (accessed on 04.02.2024).

[13] https://www.flyrotax.com/pl/products/912-ul-a-f (accessed on 05.03.2024).

[14] Idaszewska N, Szymański GM. Identification of characteristic vibration signal parameters during transport of fruit and vegetable. Vibrations in Physical Systems. 2020;31(1): 2020111-1-2020111-10. https://vibsys.put.poznan.pl/?s=Idaszewska

[15] Jałowiecki A, Fidali M, Krol A. Investigation of rolling bearing lubrication condition. Diagnostyka. 2021;22(4):51-58. https://doi.org/10.29354/diag/144123

[16] Korbicz J, Kościelny J. Modeling, diagnostics, and mastering processes. DiaSter implementation. Scientific and Technical Publishing House. Warsaw 2010.

[17] Korbicz J, Kościelny JM, Kowalczuk Z, Cholewa W. Process diagnostics. Science and Technology Publishing House. Warsaw 2002.

[18] Kozak M, Lijewski P, Fuć P. Exhaust emissions from a city bus fuelled by oxygenated diesel fuel. SAE Technical Paper 2020-01-2095. 2020. https://doi.org/10.4271/2020-01-2095

[19] Kozak M, Lijewski P, Waligórski M. Exhaust emissions from a hybrid city bus fuelled by conventional and oxygenated fuel. Energies. 2022;15(3):1123. https://doi.org/10.3390/en15031123

[20] Lijewski P, Kozak M, Fuć P, Rymaniak Ł, Ziółkowski A. Exhaust emissions generated under actual operating conditions from a hybrid vehicle and an electric one fitted with a range extender. Transport Res D-Tr E. 2020;78:102183. https://doi.org/10.1016/j.trd.2019.11.012

[21] Ma N, Han Q, Han S, Li Ch. Hierarchical re-entrant honeycomb metamaterial for energy absorption and vibration insulation. Int J Mech Sci. 2023;250:108307. https://doi.org/10.1016/j.ijmecsci.2023.108307

[22] Nowakowski T, Komorski P. Diagnostics of the drive shaft bearing based on vibrations in the high-frequency range as a part of the vehicle's self-diagnostic system. Eksploat Niezawodn. 2021;24(1):70-79. https://doi.org/10.17531/ein.2022.1.9

[23] Orczyk M, Tomaszewski F. Method of reduction of diagnostic parameters during observation on the example of a combustion engine. MATEC Web of Conferences. 2017;118: 00034-1-00034-7. https://doi.org/10.1051/matecconf/201711800034

[24] Peeters C, Leclerc Q, Antoni J, Guillaume P, Helsen J. Vibration-based angular speed estimation for multi-stage wind turbine gearboxes. J Phys Conf Ser. 2017;842:012053. https://doi.org/10.1088/1742-6596/842/1/012053

[25] Roozen NB, Urbán D, Piana EA, Glorieux C. On the use of dynamic vibration absorbers to counteract the loss of sound insulation due to mass-spring-mass resonance effects in external thermal insulation composite systems. Appl Acoust. 2021;178:107999. https://doi.org/10.1016/j.apacoust.2021.107999
[26] Sujatha C. Vibration, acoustics and strain measurement, theory and experiments. Springer 2023. https://doi.org/10.1007/978-3-031-03968-3
[27] Szymański GM, Tabaszewski M. Engine valve clearance diagnostics based on vibration signals and machine learning methods. Eksploat Niezawodn. 2020;22(2):331-339. https://doi.org/10.17531/ein.2020.2.16
[28] Szymański GM, Tomaszewski F. Diagnostics of automatic compensators of valve clearance in combustion engine with the use of vibration signal. Mech Syst Signal Pr. 2016;68-69:479-490. https://doi.org/10.1016/j.ymssp.2015.07.015
[29] Waligórski M, Batura K, Kucal K, Merkisz J. Empirical assessment of thermodynamic processes of a turbojet engine in the process values field using vibration parameters. Measurement. 2020;158:107702. https://doi.org/10.1016/j.measurement.2020.107702
[30] Waligórski M, Batura K, Kucal K, Merkisz J. Research on airplanes engines dynamic processes with modern acoustic methods for fast and accurate diagnostics and safety improvement. Measurement. 2020;154:107460. https://doi.org/10.1016/j.measurement.2019.107460
[31] Yang X-H, Kang Y, Xie X, Zhang Q, Shangguan W-B. Multilayer coupled plate-type acoustic metamaterials for low-frequency broadband sound insulation. Appl Acoust. 2023209;109399. https://doi.org/10.1016/j.apacoust.2023.109399
[32] Zhang L, Bai Z, Chen Y. Dual-functional hierarchical mechanical metamaterial for vibration insulation and energy absorption. Eng Struct. 2022;271;114916. https://doi.org/10.1016/j.engstruct.2022.114916
[33] Zhang P, Gao W, Li Y, Wei Z. Combustion parameter evaluation of diesel engine via vibration acceleration signal. Int J Engine Res. 2021;23(10):1760-1781. https://doi.org/10.1177/14680874211030878
[34] Zhu Z, Wang G, Sheng Z, Zhang Y, Xu R. Sound insulation properties of embedded co-cured composite damping sandwich panel under arbitrary boundary conditions. Mech Syst Signal Pr. 2023;204:110810. https://doi.org/10.1016/j.ymssp.2023.110810
[35] Zimroz R, Urbanek J, Barszcz T, Bartelmus W, Millioz F, Martin N. Measurement of instantaneous shaft speed by advanced vibration signal processing – application to wind turbine gearbox. Metrol Meas Syst. 2011;4:701-712. https://doi.org/10.2478/v10178-011-0066-4
[36] Zacharewicz M, Socik P, Wirkowski P, Zadrąg R, Bogdanowicz A. Evaluation of the impact of supplying a marine diesel engine with a mixture of diesel oil and n-butanol on its efficiency and emission of toxic compounds. Combustion Engines. 2023;195(4):40-47. https://doi.org/10.19206/CE-169484
[37] Żurawski PK. Optimization of the combustion chamber strength of aluminum pistons in diesel engines using the DuralBowl technology. Combustion Engines. 2023;192(1):91-96. https://doi.org/10.19206/CE-153000

Prof. Grzegorz M. Szymański, DSc., DEng. – Institute of Transport, Poznan University of Technology, Poland.
e-mail: *grzegorz.m.szymanski@put.poznan.pl*

Wojciech Misztal, DEng. – Institute of Combustion Engines and Powertrains, Poznan University of Technology, Poland.
e-mail: *wojciech.misztal@put.poznan.pl*

Prof. Marek Waligórski, DSc., DEng. – Institute of Combustion Engines and Powertrains, Poznan University of Technology, Poland.
e-mail: *marek.waligorski@put.poznan.pl*